Programmed Self-Assembly of Single Colloidal Gyroids for Chiral Photonic Crystals

Flavell, Wesley; Neophytou, Andreas; Demetriadou, Angela; Albrecht, Tim; Chakrabarti, Dwaipayan

DOI:
10.1002/adma.202211197

Document Version
Publisher's PDF, also known as Version of record

Citation for published version (Harvard):
Flavell, W, Neophytou, A, Demetriadou, A, Albrecht, T & Chakrabarti, D 2023, 'Programmed Self-Assembly of Single Colloidal Gyroids for Chiral Photonic Crystals', *Advanced Materials*, vol. 35, no. 23, 2211197. https://doi.org/10.1002/adma.202211197

ADVANCED MATERIALS
www.advmat.de

Programmed Self-Assembly of Single Colloidal Gyroids for Chiral Photonic Crystals

*Wesley Flavell, Andreas Neophytou, Angela Demetriadou, Tim Albrecht, and Dwaipayan Chakrabarti**

Gyroid structures are of extensive interest because they provide a rich platform for chiroptics as well as topological photonics. While the double-gyroid morphology as a bicontinuous structure is not uncommon in self-assembled soft materials, direct self-assembly of single-network gyroids has proven elusive. Here, an enantiomorphic pair of single-gyroid crystals comprising colloidal spheres is presented, and two distinct routes are demonstrated for programmed self-assembly of each single colloidal gyroid enantiomorph from rationally designed patchy spheres. The designer colloidal patchy spheres, which closely hew to their synthetic feasibility, are chiral, having either two staggered rectangular patches at opposite poles or four circular patches arranged in a well-defined geometry. The single colloidal gyroid, as well as its inverse structure, is shown to support a wide complete photonic bandgap in addition to exhibiting rich chiroptical properties, making them attractive chiral photonic crystals. The versatility of this single colloidal gyroid, the bottom-up routes devised here in silico, and the robustness of the design space for the chiral colloidal patchy spheres together make a strong case for single colloidal gyroids to supersede colloidal diamond, as a target for programmed self-assembly, in the quest for photonic crystals operating at optical frequencies.

1. Introduction

Gyroid structures have stimulated widespread interest across mathematical, physical, materials, and biological sciences for having intriguing structural features, rich chiroptical properties, and exotic topological physics.[1–6] The gyroid is a triply periodic minimal surface that partitions 3D space into a pair of intertwined labyrinths.[7] The skeletal graphs of these labyrinths, as shown in **Figure 1**a, define the two enantiomorphic single networks of gyroid, which have threefold connectivity at each node and characteristic ten-member rings.[1,7] The Wigner–Seitz (WS) cells of these enantiomorphs are also shown in Figure 1a, each viewed along a strut to emphasize their characteristic dihedral angles. The dihedral angles between adjacent nodes for a given enantiomorph of single network gyroid are all approximately equal to either 70.5° or 109.5°, depending on the handedness.[8] The single network gyroid structure, which has a body-centered cubic Bravais lattice with the space group $I4_132$, supports a large complete photonic bandgap (PBG),[3,9,10] and is known as a biological photonic crystal, having been found in butterfly wing scales.[11] A single-gyroid structure built from colloidal particles in the size range of hundreds of nanometers therefore promises to function as a synthetic chiral photonic crystal operating at optical frequencies.

Notwithstanding their appeal as chiral photonic crystals and metamaterials,[12,13] the single-gyroid structures have largely been ignored as targets for programmed colloidal self-assembly, mainly due to their structural complexity. Instead, colloidal diamond, in its cubic form, has drawn much attention as an attractive target for a photonic crystal at optical frequencies for nearly three decades and has often been considered as the Holy Grail of colloidal self-assembly.[14–16] The chirality of the single gyroid, however, sets it apart from other photonic structures with large complete PBGs,[10] making it a unique target for programmed self-assembly of colloidal particles with potential applications as a 3D chiral photonic crystal at optical frequencies.[13,17,18]

While the single-gyroid structures have proven elusive, the double-gyroid morphology, as a bicontinuous structure combining two subspaces of opposite handedness,[19] has been self-assembled from diverse building blocks with elements of frustration, for example, surfactants, block copolymers, and mesogens.[8,20–22] Unlike the single-gyroid structures, the double-gyroid structure is neither chiral nor supports a complete PBG. However, when the crystal system is perturbed, resulting in the breaking of inversion or time-reversal symmetry,

W. Flavell, A. Neophytou, T. Albrecht, D. Chakrabarti
School of Chemistry
University of Birmingham
Edgbaston, Birmingham B15 2TT, UK
E-mail: d.chakrabarti@bham.ac.uk
A. Demetriadou
School of Physics and Astronomy
University of Birmingham
Edgbaston, Birmingham B15 2TT, UK

The ORCID identification number(s) for the author(s) of this article can be found under https://doi.org/10.1002/adma.202211197

DOI: 10.1002/adma.202211197

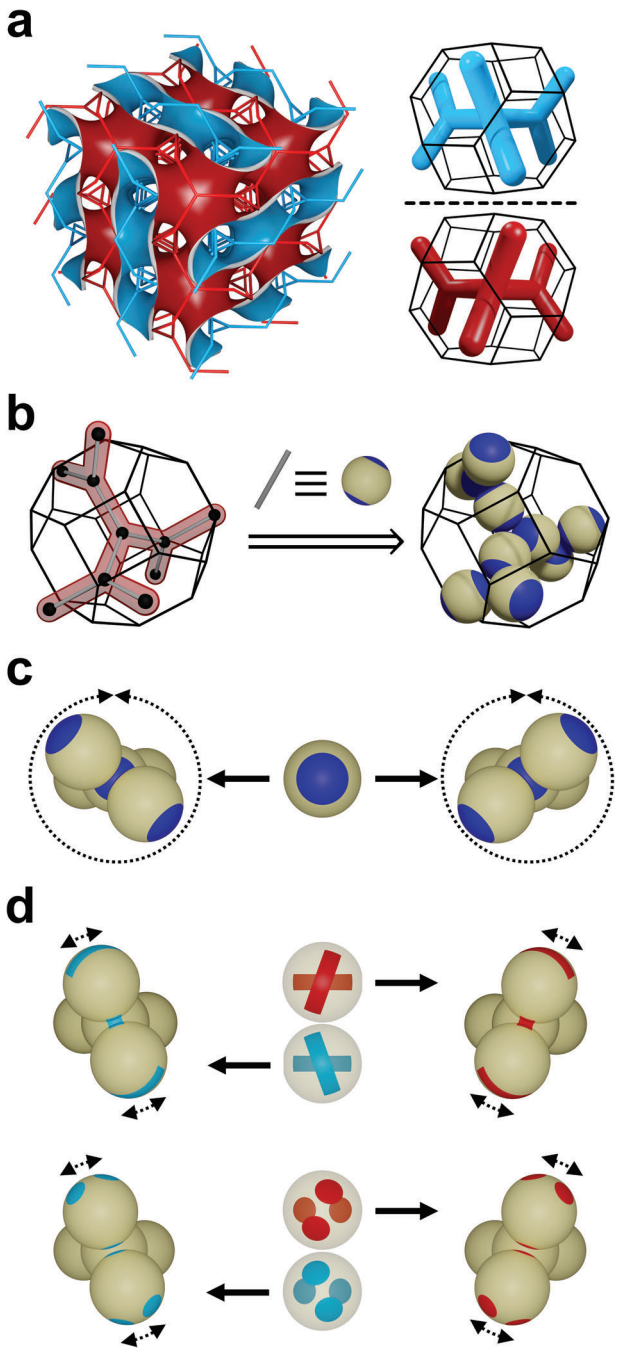

Figure 1. Rational design of colloidal patchy spheres to yield a single-gyroid crystal via self-assembly. a) 2 × 2 × 2 supercell showing the gyroid minimal surface along with its two associated skeletal graphs viewed along the [111] axis, and Wigner–Seitz cells of the single-network gyroids of opposite handedness viewed along a strut to emphasize their distinct dihedral angles. b) A single-gyroid crystal structure of a given handedness derived via discretization of the corresponding single-network gyroid. A Wigner–Seitz cell of a single network gyroid (left) is represented with its skeletal graph highlighted; the crystal structure comprising spheres (right) is obtained by replacing each edge with a triblock patchy sphere that encodes threefold connectivity at each node. c) Five-particle motif containing vertex-shared planar trimers present in single gyroids. The triblock patchy spheres with two circular patches allow for unrestricted rotation of a planar trimer relative to the other, hindering the selection of the dihedral angle required for the self-assembly of a single-gyroid structure. d) Colloidal patchy spheres to yield enantiomorphic single-gyroid crystals via self-assembly. Colloidal patchy spheres, with either two staggered rectangular patches at opposite poles (top) or four narrower circular patches arranged in a well-defined geometry (bottom) limit such rotations. The patch arrangements make the colloidal spheres chiral, opening up bottom-up routes to one or the other enantiomorph via the selection of dihedral angles.

double-gyroid-related structures can support Weyl points, where a 3D band structure locally exhibits a linear band crossing in all directions, giving rise to topological surface states.[3,5,23]

2. Results

2.1. Reverse Engineering Single Gyroids

Figure 1b presents our approach to derive a single colloidal gyroid structure from single network gyroid, using patchy spheres. Taking into consideration the WS cell of a single network gyroid structure and its corresponding skeletal graph, colloidal building blocks—specifically triblock patchy spheres with circular patches at opposite poles—can be envisaged to replace each edge in the network. Advances in colloid synthesis have made triblock patchy spheres especially attractive building blocks for programmed colloidal self-assembly.[24,25] The width of the circular patches on either pole can be optimized to allow for contacts with only two other patches, as shown in Figure S1a, Supporting Information, thereby giving rise to a trigonal unit centered on each node. In a characteristic five-particle motif, containing two vertex-shared planar trimers, the circular patches, however, allow for unrestricted rotation of one trimer with respect to the other, as shown schematically in Figure 1c. As a result, we observe that triblock patchy particles with two circular patches, despite possessing patch widths that encode threefold connectivity, do not self-assemble into a gyroid structure; instead a crystal structure comprising stacked kagome planes is self-assembled (see Section A and Figure S1, Supporting Information).

Faced with this issue, we conceived two particle designs, as illustrated in Figure 1d. Both the designs restrict the relative rotation of vertex-shared planar trimers and thus enforce the selection of the dihedral angles required to assemble a single-gyroid structure from colloidal spheres. One route involves the replacement of the two circular patches at opposite poles of spherical particles with two staggered rectangular ones. An alternative route involves spherical patchy particles decorated with four narrower circular patches to encode the five-particle structural motif. In the latter route, in essence, each rectangular patch is replaced by two circular ones. Both bottom-up routes are designed in the context of synthetic advances, which can fabricate rectangular patches on opposite poles[26] and four circular patches[24] using variants of the glancing-angle deposition technique.

Figure 2a illustrates the critical parameters that describe the patch shape, size and relative arrangement for the patchy particles with staggered rectangular patches at opposite poles. We developed an effective pair potential for these particles based on the concepts of the widely used Kern–Frenkel model.[27] In this new model, each rectangular patch is characterized by two half-opening angle values, θ_p and ϕ_p, giving the latitudinal and longitudinal bounds of each patch, respectively. The relative orientation between the two patches is described by the skew angle

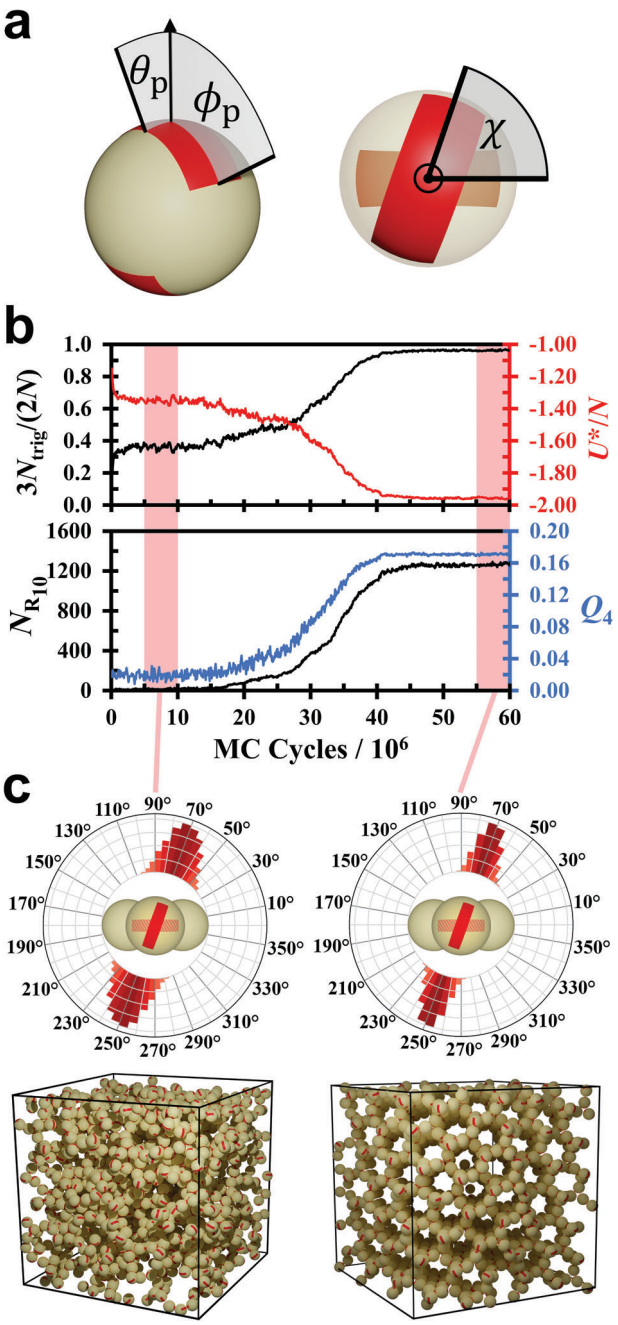

Figure 2. Self-assembly of single colloidal gyroids from particles with two rectangular patches. a) Parametrization of the rectangular patches on a colloidal patchy sphere, showing the two half-angles, θ_p and ϕ_p, which define the surface coverage and geometry of each patch, and the skew angle, χ, that defines the relative orientation of the patches. b) Evolution of the number of trigonal planar clusters, N_{trig}, (black line), the potential energy per particle, U^*/N, (red line), the global Steinhardt bond-order parameter, Q_4, (blue line), and the number of ten-member rings, $N_{R_{10}}$, (black line) for a system of $N = 1500$ patchy particles, with two equal-size staggered rectangular patches at opposite poles with half-opening angles $\theta_p = 10°$, $\phi_p = 44°$ and skew parameter $\chi = 70.5°$, at a density $\rho^* = 0.3$, following one-step quenching from a temperature of $T^* = 1$ to $T^* = 0.11$. c) Polar histograms (top) of the dihedral angles between the nodes of threefold connectivity over two intervals of 5 million Monte Carlo cycles at the pre- and post-nucleation stages, as indicated by the red shading in (b), and representative configurations (bottom) within the two intervals.

χ, which is critical to the selection of dihedral angles. See Section B and Figures S2– S5, Supporting Information for more details on the model. We envisage that the conceptual development of colloidal particles with rectangular patches and their effective interactions presented here will drive the synthesis of the next generation of patchy colloidal particles with non-circular patches. For example, spherical colloidal particles with triangular patches were considered in simulations targeting diamond-related crystals via patterning symmetry,[28] and have since been synthesized experimentally.[29]

2.2. Programmed Self-Assembly

We carried out Monte Carlo simulations for the designer patchy particles with two staggered rectangular patches at opposite poles to investigate the programmed self-assembly of single colloidal gyroid. In these simulations, we considered systems of $N = 1500$ particles over a range of patch geometries with $\chi = 70.5°$ and $\chi = 109.5°$ at a density of $\rho^* = 0.3$. Note that any choice of χ that is not 0° or 90° makes the patchy particles chiral. Figure 2b (top) shows the evolution of the number of trigonal planar clusters, N_{trig}, and the potential energy per particle, U^*/N, for a system with $\chi = 70.5°$, $\theta_p = 10°$ and $\phi_p = 44°$ along a trajectory following a one-step quench from a temperature of $T^* = 1$ to $T^* = 0.11$. The rapid change in N_{trig}, concomitant with the change in potential energy, suggests a first-order phase transition. The evolution of the global Steinhardt bond-order parameter Q_4,[30] as described in Experimental Section, along the trajectory, is shown in Figure 2b (bottom), together with the number of ten-member rings ($N_{R_{10}}$) present in the system. The data confirm the growth of crystalline order, which is clearly driven by the formation of ten-member rings. We therefore infer that the chirality transfer from the single-particle level to an enantiomorphic crystal occurs via the formation of ten-member rings. Figure 2c shows polar histograms of the dihedral angles between the nodes of threefold connectivity for two equal intervals at the pre- and post-nucleation stages. We find that the dihedral angles are restricted to a small range around the ideal angle even at the pre-nucleation stage, showing our design principles in action. This distribution of dihedral angles is distinct from what we observe for circular patches, as shown in Figure S1c, Supporting Information. The distribution becomes narrower around the ideal angle post-nucleation, as the size of fluctuations becomes limited. Figure 2c also shows representative fluid and crystalline configurations within the intervals.

We observe the crystallization of colloidal patchy particles with two staggered rectangular patches at opposite poles into a single colloidal gyroid structure following a one-step quench for systems of $N = 768$ particles with a range of patch geometries, extending at least the rectangular parameter space defined by $\theta_p = [6°–14°]$ and $\phi_p = [36°–50°]$ (see Section C and Figure S6, Supporting Information). To determine the robustness of the crystallization of single colloidal gyroid, with respect to the choice of the skew angle χ, we carried out a series of Monte Carlo simulations using systems of $N = 768$ particles at a density of $\rho^* = 0.3$ with $\theta_p = 10°$, $\phi_p = 44°$ and $\chi = [60°–120°]$ (with a resolution of 2°). **Figure 3**a shows the final ten-member ring counts, $N_{R_{10}}$, and global Steinhardt bond-order parameter values, Q_4, for

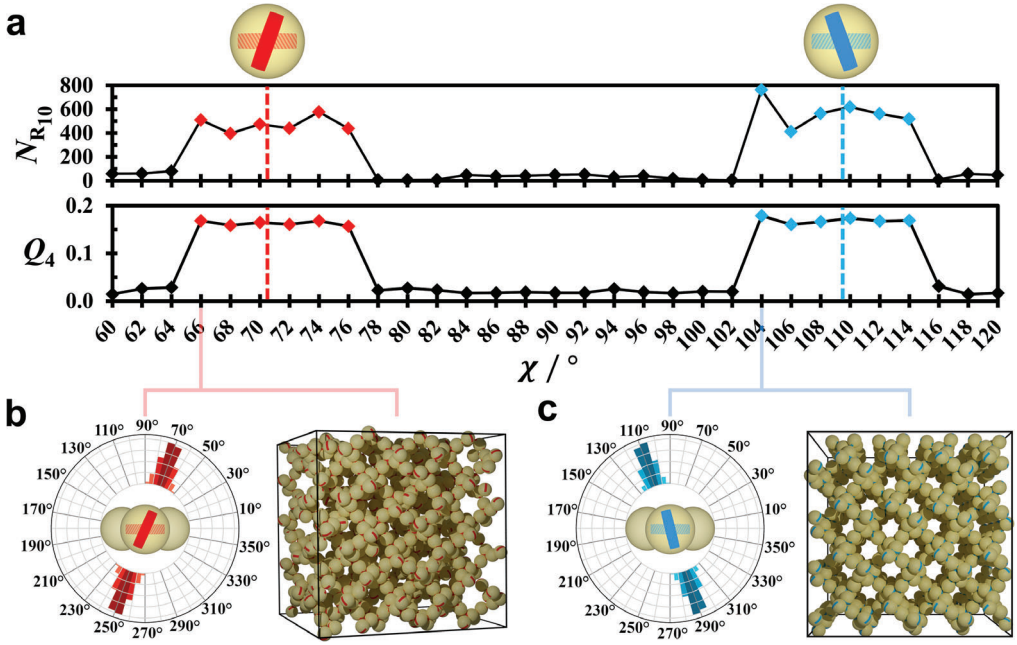

Figure 3. Robustness of the skew angle space for crystallizing single colloidal gyroid structures. a) Final ten-member ring counts, $N_{R_{10}}$, and global Steinhardt bond-order parameter values, Q_4, as a function of skew angle, χ, for systems of $N = 768$ particles with two rectangular patches ($\theta_p = 10°$, $\phi_p = 44°$) after the temperature is dropped from $T^* = 1$ to $T^* = 0.11$. Red and blue dashed lines indicate the ideal χ values for right and left-handed gyroid respectively, and red and blue points indicate corresponding crystalline configurations. b,c) Inter-trimer dihedral angle distributions (taken over the last 10 million Monte Carlo cycles), and final configurations for the $\chi = 66°$ (b) and $\chi = 104°$ (c) systems.

each system after equilibration upon quenching from $T^* = 1$ to $T^* = 0.11$. The plots clearly show the two regions, which yield enantiomorphic single colloidal gyroid crystals in the ranges $\chi =$ [66°–76°] and [104°–114°]. Figure 3b,c shows the dihedral angle distributions, and final configurations for the $\chi = 66°$ and $\chi = 104°$ systems, respectively.

The selection of dihedral angles can also be encoded in particles with four circular patches, where each patch is predisposed to form a single contact and centered on each of the four points of contact formed by the central particle in the desired five-particle motif, as shown in **Figure 4**a. Figure 4b shows the parametrization we used to define such a four-patch particle. In this scheme, each hemisphere has two circular patches, each with a half-opening angle of α. The centers of these pairs of patches subtend an angle β at the center of the colloidal sphere, and the relative orientation of the patch pairs is defined in a similar manner as in the rectangular patch case, via the skew angle χ.

We carried out a series of Monte Carlo simulations with systems of these four-patch particles ($\beta = 60°$, $\chi = 70.5°$, and 109.5°) with $\alpha = 8°$, 10°, 15°, 20°, 22°. We observe the self-assembly of a single-gyroid structure for $\alpha = 8°$, 10°, 15°, 20° following a one-step quench from $T^* = 1$ to as high as $T^* = 0.108$, 0.115, 0.123, and 0.125, respectively. Figure 4c shows the evolution of N_{trig}, U^*/N, Q_4, and $N_{R_{10}}$, for a system of $N = 768$ four-patch particles with $\alpha = 10°$, after the temperature is dropped to $T^* = 0.113$. Figure 4d shows a representative crystalline configuration.

We systematically assessed the robustness of the design space for the colloidal patchy particles in terms of the patch attributes to crystallize into a single colloidal gyroid structure. As described in Section C1, Supporting Information, the crystallization is observed for the two-patch particles over a sufficiently large parameter space for the patch coverage (Figure S6, Supporting Information), in addition to the skew angle. We note that spontaneous crystallization for particles with a smaller patch coverage takes place in our simulations at a lower temperature, for both two-patch and four-patch particles, due to a smaller bonding volume. The crystallization is also found to show remarkable tolerance to polydispersity in the angular parameters, θ_p, ϕ_p, and χ, defining the coverage and the relative orientations of the patches in the case for two-patch particles (Figure S7– S9, Supporting Information).

Although our focus was on assessing the robustness of the design space in terms of the patch attributes, we also investigated the effects of polydispersity in particle size. Our simulations with two-patch particles up to 5% size polydispersity, which is well within the reach of state-of-the-art synthesis of triblock patchy particles,[24] show that the self-assembly into single colloidal gyroid is sufficiently tolerant to polydispersity in particle size as well (see Section C1 and Figure S10, Supporting Information). For the four-patch particles (see Section C2, Supporting Information), we find a sufficiently large parameter space for the opening angle β to support crystallization into a single colloidal gyroid structure (Figure S11, Supporting Information), and demonstrate significant tolerance to polydispersity in patch size for fixed patch arrangements (Figure S12, Supporting Information). We have so far presented data from Monte Carlo simulations carried out at a density of $\rho^* = 0.3$, which is close to the ideal density of the perfect crystal. Additionally, we find that the self-assembly of single colloidal gyroid occurs across a wide range of densities (see Figure S13, Supporting Information).

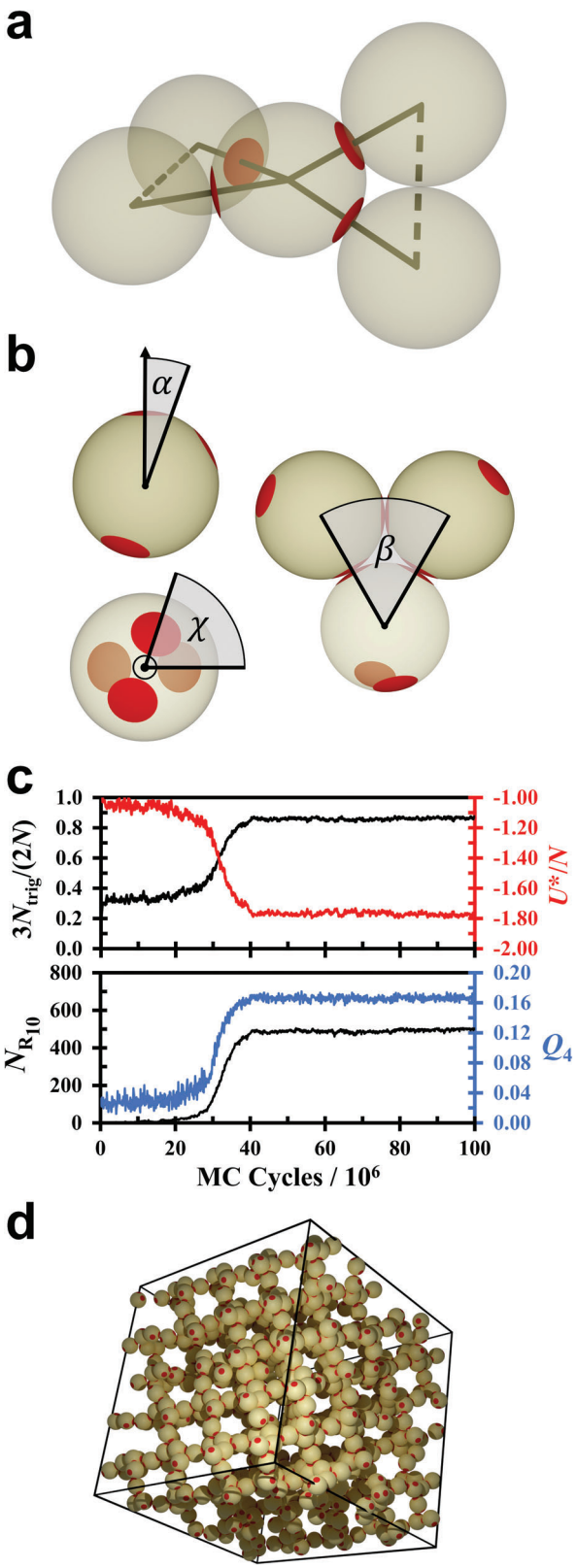

Figure 4. Self-assembly of single colloidal gyroid from four-patch particles. a) Spherical patchy particles with four circular patches to encode the characteristic five-particle structural motif of the target single-gyroid crystal structure. The patches are arranged so that the bonds to the central particle pass through the centers of the patches. The dashed lines show the bonds which complete the two planar trigonal units. b) Parametrization of the size and arrangement of the patches for a four-patch spherical particle with the set of angles α, β, and χ. c) Evolution of the number of trigonal planar units, N_{trig}, the potential energy per particle, U^*/N, the global Steinhardt bond-order parameter, Q_4, and the number of ten-member rings, $N_{R_{10}}$, for a system of $N = 768$ four-patch particles, with $\alpha = 10°$, $\beta = 60°$, $\chi = 109.5°$, following one-step quenching from $T^* = 1$ to $T^* = 0.113$. d) Representative crystalline configuration.

2.3. Chiroptical Properties

Having established that our designer patchy particles offer reliable bottom-up routes to single colloidal gyroid crystals, we determined whether the resulting structures, like the single network gyroid,[10,13,31] can function as chiral photonic crystals. **Figure 5**a shows the relative gap width, $\Delta f/f_m$ expressed as a percentage, of the direct single colloidal gyroid structure (dielectric spheres in air) as a function of the refractive index contrast ($n_c = n_h/n_l$). For the direct structure, we consider the maximum packing scenario (i.e., where the dielectric spheres are touching), which corresponds to a density of $\rho^* = 9\sqrt{6}/64 \approx 0.34$. We find that a complete PBG opens up for $n_c \approx 2.7$, which could potentially be realized with titania particles in order to open a PBG in the visible.[32] However, it is possible to further lower the required refractive-index contrast by depositing materials onto the surfaces of the particles, effectively increasing the dielectric filling fraction.[16,33] This "swelling" of the particles can also be used to fabricate the inverse structure, which involves backfilling the voids of the direct lattice with a high refractive-index material, after which the original material can be removed leaving air in its place.[16] The inverse single colloidal gyroid structure, composed of "air spheres" with a diameter of twice the original diameter (as shown by the inset of Figure 5b), is a close approximation to single network gyroid.[10,13] This is apparent from the fact that a complete PBG opens up for this inverse structure for $n_c \approx 2.2$, as shown in Figure 5b, similar to what has previously been reported for single network gyroid.[10,13] Representative photonic band structures for both the direct and inverse single-gyroid structures presented here are shown in Figures 5c and 5d, respectively, for the refractive index contrast $n_c = 3$, showing the presence of a complete PBG in each case.

We note that both the direct and inverse structures in this case are single-gyroid-like structures, but are of opposite chirality. This is not immediately evident when comparing the dispersion relations in Figures 5e and 5f, where we show the band structures along the $\Gamma \rightarrow X$ direction for the conventional unit cells of the direct and inverse structures, respectively, with $n_c = 3$. However, we are able to determine the handedness of the bands using the circular dichroism index ($C \in [-1, 1]$),[31,34] which measures the preference of Bloch modes to couple to right-handed ($C \approx 1$) or left-handed ($C \approx -1$) light (see Experimental Section). A close comparison between the left panels of Figure 5e,f reveals that the handedness of the bands for the direct and inverse structures is flipped relative to one another, highlighting that the two structures are indeed of opposite chirality. We confirm the difference in the chirality of the two structures by calculating the transmittance spectra for right-circularly polarized (RCP) and left-circularly polarized (LCP) plane waves normally incident to a finite slab of the direct and inverse gyroid crystals along the [100]

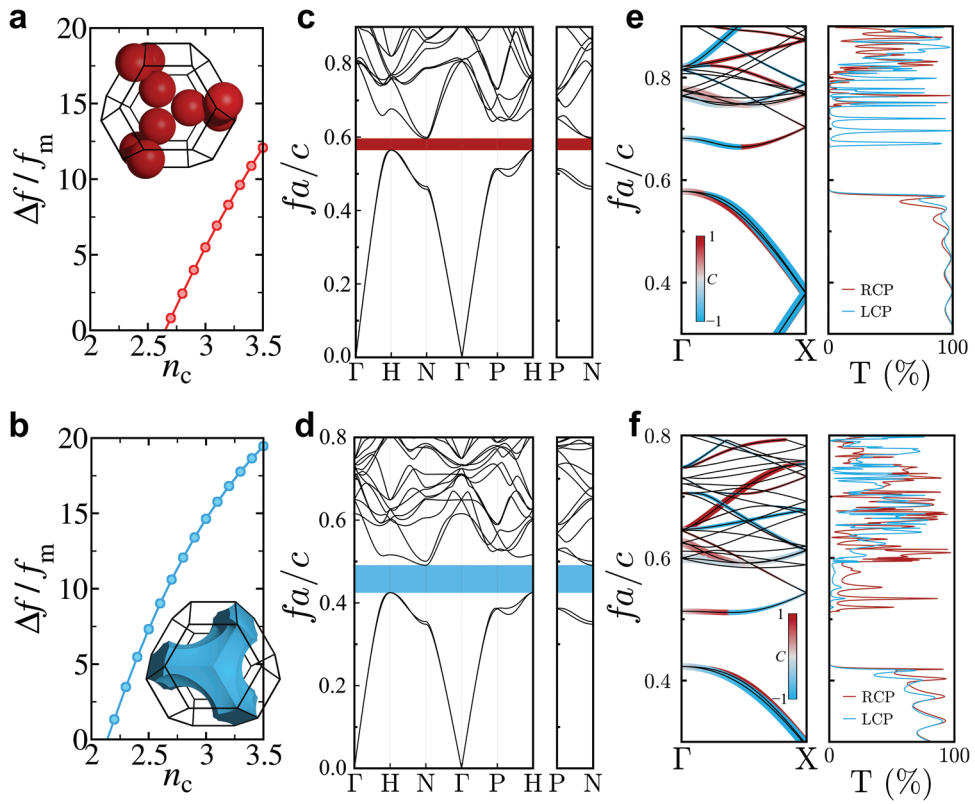

Figure 5. Chiroptical properties for single colloidal gyroid structures. a,b) Dependence of the relative gap width ($\Delta f/f_m$), expressed as a percentage, on the refractive index contrast (n_c) for the direct (a) and inverse (b) single colloidal gyroid structures. c,d) Photonic band structures of the direct (c) and inverse (d) gyroid structures with $n_c = 3$, showing complete PBGs of ≈5% and ≈15%, respectively. e,f) The left panels show the photonic band structures of the conventional unit cells of the direct (e) and inverse (f) gyroid structures with $n_c = 3$ along the $\Gamma \rightarrow X$ direction (which corresponds to the $\Gamma \rightarrow H$ direction in the primitive unit cell). The color of the lines in both band structures reflects the circular dichroism index (C), where right-circularly polarized (RCP) is red, left-circularly polarized (LCP) is blue, and unpolarized is black, and their thickness is proportionate to the coupling constant β (see Experimental Section). The right panels show the transmittance spectra for RCP (red) and LCP (blue) plane waves normally incident to a finite slab of the direct (e) and inverse (f) gyroid crystals with $n_c = 3$ along the [100] direction. For all calculations the direct colloidal gyroid structure is composed of touching dielectric spheres as shown by the inset of (a). At the limit of touching spheres the density of the colloidal gyroid crystal is $\rho^* = 9\sqrt{6}/64 \approx 0.34$ and the edge length of the corresponding conventional unit cell is $a = 4d\sqrt{6}/3$, d being the diameter of the particles. Again, for all calculations the inverse colloidal gyroid structure is composed of air spheres with a radius of $r = d^2/a$. The inset of (b) visually highlights that the inverse structure is a gyroid network of opposite handedness relative to the direct structure.

direction, as shown in the right panels of Figure 5e and 5f, respectively. For the direct structure, we observe a broad dip in the transmittance of RCP light across frequencies spanning both the unpolarized stop gap and the dichroic bandgap of the gyroid,[31] while the inverse structure displays a broad dip in the transmittance of LCP light. See Section D and Figure S14, Supporting Information for supplementary discussion.

3. Conclusions

We have achieved programmed self-assembly of single colloidal gyroid structures from two distinct types of colloidal patchy spheres, one with two equal-size staggered rectangular patches at opposite poles and the other with four equal-size circular patches arranged in a well-defined geometry. The shape, size and arrangements of the patches encode the threefold connectivity at each node and the selection of the gyroid dihedral angle between adjacent nodes—which is critical to the elimination of competing structures in preference to single colloidal gyroid. For patchy particles with rectangular patches, we developed a pair potential, based on the concepts of the widely used Kern–Frenkel model for patchy particles with circular patches but adapted to the modified patch geometry. This model can be used to study a variety of quadrilateral patches, and easily modified to study more complex patch geometries.

Our simulations demonstrate enantiomorphic crystallization of single colloidal gyroid, where the chirality transfer from the single-particle level is driven by the formation of ten-member rings. We establish that crystallization of the designer building blocks considered here is considerably robust with respect to deviations from the ideal patch arrangement, which further lends our design principles to experimental validation. The single-gyroid crystals built from chiral colloidal spheres support a complete PBG at relatively low refractive index contrasts accessible to colloidal materials, and exhibit rich chiropical effects, thus opening the door for developing novel photonic materials with applications in light-harvesting technology and sensing among others. We envisage the self-assembly routes to single colloidal

gyroid established here to drive the field of colloidal self-assembly with the exploration of novel optical effects, emerging from a complex interplay of chirality, photonics and topology.[3,4,23,35,36] This work thus paves the way for new self-assembly routes toward building chiral and topological devices operating at optical frequencies,[5,37] as well as emulating nature's design of chiral photonic structures.[38,39]

4. Experimental Section

Monte Carlo Simulations: Monte Carlo simulations were performed with systems of N particles at a number density of $\rho^* = Nd^3/V = 0.3$ (where d is the diameter of the hard-core and V is the volume of the system) in the canonical ensemble, within a cubic simulation box under periodic boundary conditions. The orientational degrees of freedom were represented using quaternions, and each Monte Carlo cycle consisted of N single-particle moves. Each system was equilibrated at $T^* = k_B T/\epsilon = 1$ (where k_B is the Boltzmann constant and ϵ is the well-depth of the patchy interactions) before subject to quenching. In the present study, reduced units were used: the length in units of d, the energy ($U^* = U/\epsilon$, where U is the potential energy) in units of ϵ, the temperature in units of ϵ/k_B, with the Boltzmann constant k_B taken to be equal to one. The details of the structural analysis performed along the Monte Carlo trajectories are provided in Section E, Supporting Information.

Photonic Band Structure Calculations: The photonic band structures of the crystal structures were calculated using the open-access software package `MIT Photonic Bands` (`MPB`).[40] The software computes fully vectorial eigenmodes of Maxwell's equations with periodic boundary conditions by a preconditioned conjugate-gradient minimization of the block Rayleigh quotient in a plane wave basis. For all calculations,it was assumed that the crystal structures considered were composed of an isotropic and lossless material that had a linear response to an applied electromagnetic field. `MPB` takes the fractional coordinates, geometry and dielectric constant of the particles, and the primitive lattice basis of the crystal structure as input. A resolution of 32 mesh points per a unit was used for all calculations, where $a = 4d\sqrt{6}/3$ is the edge length of the conventional unit cell of the colloidal gyroid crystal composed of touching spheres.

Circular polarization analysis was performed on the photonic band structures of the gyroid crystals by calculating the circular dichroism index (C) and the coupling index (β) of the eigenmodes, where[31,34]

$$C = \mathrm{sgn}(\mathbf{q}\cdot\nabla_{\mathbf{k}} f_n)\left(\frac{C^+_{\mathbf{k},n} - C^-_{\mathbf{k},n}}{C^+_{\mathbf{k},n} + C^-_{\mathbf{k},n}}\right) \tag{1}$$

is defined where n is the band index, $\mathbf{k}$ is the Bloch wave vector, $\nabla_{\mathbf{k}} f_n$ is the group velocity and $C^{\pm}_{\mathbf{k},n}$ is the overlap integral between Bloch modes and a circularly polarized plane wave with wave vector $\mathbf{q} \parallel \mathbf{k} = k\hat{\mathbf{b}}$. The overlap integral is defined as[31,34]

$$C^{\pm}_{\mathbf{k},n} = \frac{\left|\int\int_P (\hat{\mathbf{a}} \pm i\hat{\mathbf{c}})\cdot \mathbf{H}_{\mathbf{k},n}(P)\right|^2}{\left|\int\int_P (\hat{\mathbf{a}} \pm i\hat{\mathbf{c}})\right|^2 \left|\int\int_P \mathbf{H}_{\mathbf{k},n}(P)\right|^2} \tag{2}$$

where $\mathbf{H}_{\mathbf{k},n}$ corresponds to a magnetic eigenmode. The integrals are performed over a plane P that is perpendicular to $\hat{\mathbf{b}}$ and the unit vectors $\hat{\mathbf{a}}$ and $\hat{\mathbf{c}}$ are in the plane. Additionally, the center of the plane was fixed to be at the origin. For each eigenmode a handedness can be assigned: if $C > 0.5$ it is right-handed (RH), if $C < -0.5$ it is left-handed (LH) and a mode remains unassigned otherwise. Additionally, the coupling index can be defined

$$\beta = C^+_{\mathbf{k},n} + C^-_{\mathbf{k},n} \tag{3}$$

which measures the degree of coupling between an incident plane wave of either polarization and the corresponding eigenmode. In plots of the photonic band structures and the circular dichroism index the color of the symbols reflects the value of the circular dichroism index and the size of the symbols was proportional to the coupling index.

Transmittance Spectra Calculations: Transmittance spectra for circularly polarized light incident on finite slabs of colloidal gyroid were calculated using the freely available finite-difference time domain (FDTD) package `MEEP`.[41] For each simulation a finite slab of five (conventional) unit cells of colloidal gyroid, where periodic boundaries were imposed along the $\hat{\mathbf{x}}$ and $\hat{\mathbf{z}}$ directions of the simulation cell. The simulation cell was defined with a Yee grid of 42 points per unit cell and a size of $1 \times 15 \times 1$ unit cells, where perfectly matched layers were positioned on either side of the simulation cell where periodic boundaries were not imposed. A Gaussian source was defined on one side of the colloidal gyroid slab, with energy flux measured on the other side. Circularly-polarized sources were generated by overlapping two linearly-polarized sources which were 90° out of phase with one another.

Supporting Information

Supporting Information is available from the Wiley Online Library or from the author.

Acknowledgements

W.F. and A.N. gratefully acknowledge support from the University of Birmingham. A.N. also thanks support from the Institute of Advanced Studies of the University of Birmingham. The authors thank Daan Frenkel and Francesco Sciortino for stimulating discussions. A.D. acknowledges support from the Royal Society University Research Fellowship URF/R1/180097, the Royal Society Research Fellows Enhancement Award RGF/EA/181038 and Royal Society Research grant RGS\R1\211093. A.D. and D.C. acknowledge support from the EPSRC CDT in Topological Design EP/S02297X/1. The authors acknowledge the use of the BlueBEAR HPC service of the University of Birmingham.

Conflict of Interest

The authors declare no conflict of interest.

Data Availability Statement

The data that support the findings of this study are available from the corresponding author upon reasonable request.

Keywords

chiral colloids, chiral photonic crystals, colloidal self-assembly, gyroid structures, patchy colloids

Received: November 30, 2022
Revised: February 8, 2023
Published online: April 17, 2023

[1] S. T. Hyde, M. O'Keeffe, D. M. Proserpio, *Angew. Chem., Int. Ed.* **2008**, *47*, 7996.

[2] S. T. Hyde, G. E. Schröder-Turk, *Interface Focus* **2012**, *2*, 529.
[3] L. Lu, L. Fu, J. D. Joannopoulos, M. Soljačić, *Nat. Photonics* **2013**, *7*, 294.
[4] L. Lu, J. D. Joannopoulos, M. Soljačić, *Nat. Phys.* **2016**, *12*, 626.
[5] M. Fruchart, S.-Y. Jeon, K. Hur, V. Cheianov, U. Wiesner, V. Vitelli, *Proc. Natl. Acad. Sci. USA* **2018**, *115*, E3655.
[6] H. Wang, S. Lee, J. S. Du, B. E. Partridge, H. F. Cheng, W. Zhou, V. P. Dravid, B. Lee, S. C. Glotzer, C. A. Mirkin, *Nat. Mater.* **2022**, *21*, 580.
[7] A. H. Schoen, *Infinite Periodic Minimal Surfaces without Self-Intersections*, National Aeronautics and Space Administration, Washington, D.C., USA **1970**.
[8] X. Feng, C. J. Burke, M. Zhuo, H. Guo, K. Yang, A. Reddy, I. Prasad, R.-M. Ho, A. Avgeropoulos, G. M. Grason, E. L. Thomas, *Nature* **2019**, *575*, 175.
[9] M. Maldovan, A. M. Urbas, N. Yufa, W. C. Carter, E. L. Thomas, *Phys. Rev. B* **2002**, *65*, 165123.
[10] H. Men, K. Y. K. Lee, R. M. Freund, J. Peraire, S. G. Johnson, *Opt. Express* **2014**, *22*, 22632.
[11] K. Michielsen, D. G. Stavenga, *J. R. Soc. Interface* **2008**, *5*, 85.
[12] S. S. Oh, A. Demetriadou, S. Wuestner, O. Hess, *Adv. Mater.* **2012**, *25*, 612.
[13] J. A. Dolan, B. D. Wilts, S. Vignolini, J. J. Baumberg, U. Steiner, T. D. Wilkinson, *Adv. Opt. Mater.* **2015**, *3*, 12.
[14] K. M. Ho, C. T. Chan, C. M. Soukoulis, *Phys. Rev. Lett.* **1990**, *65*, 3152.
[15] M. Maldovan, E. L. Thomas, *Nat. Mater.* **2004**, *3*, 593.
[16] M. He, J. P. Gales, E. Ducrot, Z. Gong, G.-R. Yi, S. Sacanna, D. J. Pine, *Nature* **2020**, *585*, 524.
[17] M. D. Turner, M. Saba, Q. Zhang, B. P. Cumming, G. E. Schröder-Turk, M. Gu, *Nat. Photonics* **2013**, *7*, 801.
[18] R. K. Cersonsky, J. Antonaglia, B. D. Dice, S. C. Glotzer, *Nat. Commun.* **2021**, *12*, 2543.
[19] L. E. Scriven, *Nature* **1976**, *263*, 123.
[20] K. Fontell, *Colloid Polym. Sci.* **1990**, *268*, 264.
[21] F. S. Bates, G. H. Fredrickson, *Phys. Today* **1999**, *52*, 32.
[22] S. Kutsumizu, *Isr. J. Chem.* **2012**, *52*, 844.
[23] L. Lu, Z. Wang, D. Ye, L. Ran, L. Fu, J. D. Joannopoulos, M. Soljačić, *Science* **2016**, *349*, 622.
[24] Q. Chen, E. Diesel, J. K. Whitmer, S. C. Bae, E. Luijten, S. Granick, *J. Am. Chem. Soc.* **2011**, *133*, 7725.
[25] Q. Chen, S. C. Bae, S. Granick, *Nature* **2011**, *469*, 381.
[26] A. B. Pawar, I. Kretzschmar, *Langmuir* **2009**, *25*, 9057.
[27] N. Kern, D. Frenkel, *J. Chem. Phys.* **2003**, *118*, 9882.
[28] F. Romano, F. Sciortino, *Nat. Commun.* **2012**, *3*, 975.
[29] M. He, J. P. Gales, X. Shen, M. J. Kim, D. J. Pine, *Langmuir* **2021**, *37*, 7246.
[30] P. J. Steinhardt, D. R. Nelson, M. Ronchetti, *Phys. Rev. B* **1983**, *28*, 784.
[31] M. Saba, M. Thiel, M. D. Turner, S. T. Hyde, M. Gu, K. Grosse-Brauckmann, D. N. Neshev, K. Mecke, G. E. Schröder-Turk, *Phys. Rev. Lett.* **2011**, *106*, 103902.
[32] G. Subramania, K. Constant, R. Biswas, M. Sigalas, K.-M. Ho, *Appl. Phys. Lett.* **1999**, *74*, 3933.
[33] É. Ducrot, J. Gales, G.-R. Yi, D. J. Pine, *Opt. Express* **2018**, *26*, 30052.
[34] J. C. W. Lee, C. Chan, *Opt. Express* **2005**, *13*, 8083.
[35] M. Y. B. Zion, X. He, C. C. Maass, R. Sha, N. C. Seeman, P. M. Chaikin, *Science* **2017**, *358*, 633.
[36] B.-Y. Xie, H.-F. Wang, X.-Y. Zhu, M.-H. Lu, Z. D. Wang, Y.-F. Chen, *Opt. Express* **2018**, *26*, 24531.
[37] Y.-J. Kim, J.-B. Moon, H. Hwang, Y. S. Kim, G.-R. Yi, *Adv. Mater.* **2023**, *35*, 2203045.
[38] I. I. Smalyukh, *Adv. Mater.* **2021**, *33*, 2001228.
[39] J. Lv, D. Ding, X. Yang, K. Hou, X. Miao, D. Wang, B. Kou, L. Huang, Z. Tang, *Angew. Chem., Int. Ed.* **2019**, *58*, 7783.
[40] S. G. Johnson, J. D. Joannopoulos, *Opt. Express* **2001**, *8*, 173.
[41] A. F. Oskooi, D. Roundy, M. Ibanescu, P. Bermel, J. D. Joannopoulos, S. G. Johnson, *Comput. Phys. Commun.* **2010**, *181*, 687.